Appl. Phys. B 78, 885–890 (2004)
DOI: 10.1007/s00340-004-1429-2

Applied Physics B
Lasers and Optics

T. NISHIKAWA[1,✉]
S. SUZUKI[1]
Y. WATANABE[1]
O. ZHOU[2]
H. NAKANO[1]

Efficient water-window X-ray pulse generation from femtosecond-laser-produced plasma by using a carbon nanotube target

[1] NTT Basic Research Laboratories, NTT Corporation, 3-1 Morinosato Wakamiya, Atsugi-shi, Kanagawa 243-0198, Japan
[2] University of North Carolina, Chapel Hill, North Carolina 27599, USA

Received: 27 October 2003 /
Revised version: 26 December 2003
Published online: 12 March 2004 •

ABSTRACT We adopt a multiwalled carbon nanotube target to increase the efficiency of water-window and K_α X-ray pulse conversion from femtosecond-laser-produced plasma. The diameter of the carbon nanotubes is around 30 nm and the length is about 12-μm. The X-ray fluence enhancement in the water-window region is sevenfold compared with a conventional carbon plate target. Further enhancement can be expected by optimizing the size of the carbon nanotubes. Soft X-ray pulse duration is 26 ps. It is also found that the K_α X-ray line emission from the Si substrate of the carbon nanotube target was enhanced. This result indicates that by covering various solid materials with carbon nanotubes, enhanced short K_α X-ray pulses with the corresponding wavelength can be obtained. These results show that carbon nanotubes are very attractive as a target for femtosecond laser-produced-plasma X-ray sources in single-shot X-ray microscopy and time-resolved X-ray diffraction.

PACS 52.50.Jm; 52.38.-r; 52.38.Ph; 68.37.Yz; 78.67.-n

1 Introduction

Laser-produced plasma X-ray sources are compact and inexpensive and provide intense short X-ray pulses that make single-shot measurements possible. One promising application area is X-ray microscopic imaging in the water-window region (2.3–4.4 nm) of living cells. Due to the large absorption differences between carbon and oxygen in the water-window region, the natural contrast between protein and water can be obtained. In addition, short single-pulse exposure measurements allow us to obtain images of living cells before structural changes of the specimen caused by the radiation process degrade resolution. Laser produced plasma X-ray pulse generation in the water-window region has been demonstrated with a Mylar and ethanol target. However, obtaining the short X-ray pulses sufficient for single shot X-ray microscopy requires further improvement of conversion efficiency in laser produced plasma X-ray sources.

✉ Fax: +81-46/270-2361, E-mail: nisikawa@will.brl.ntt.co.jp

2 Nanostructure-array targets

Nanostructured targets are attractive for enhancing intensity of the X-ray pulse generated from laser-produced plasma. Efficient hot electron, fast ion, and thermonuclear neutron production with moderate laser intensity has also been reported. Several types of nanostructured targets have been reported. These include grating [1, 2], colloidal [1–3], porous [4, 5], velvet [6], and rough surface [7–10] targets. In hard X-ray energy regions (> 1 keV), large X-ray intensity enhancement of one or two orders of magnitude has been achieved while keeping the X-ray pulse duration short. But in the soft X-ray energy regions(< 0.2 keV), the attained X-ray conversion efficiency enhancement has been small or X-ray pulse duration expands too much [3, 5, 6]. The 14-fold soft X-ray intensity enhancement compared with a flat surface target was obtained with a colloidal Ni target but soft X-ray pulse duration expands to 70 ps [6]. The short soft X-ray pulse duration of 25 ps was obtained with a Ni coated grating target and a Ni velvet target but the soft X-ray intensity enhancement was only fourfold [6].

In order to improve this situation, we adopted the nanostructure-array targets. One is an alumina nanohole-array target [11, 12] and the other is a gold nanocylinder-array target [13]. The new features of these targets are a deep nanostructure aligned to the laser incident direction and nanometer-sized spaces. Like previously reported nanostructured targets, these targets also have a low average density but a high local density structure. The large surface area and thin nanowall structure enlarges the region of interaction with the laser pulse, the nanospaces promote electron oscillation and ion collisions, and the low thermal conductivity increases plasma temperature.

Figure 1 shows a top-view scanning electron microscope (SEM) image of the alumina nanohole-array target with nanohole interval of 100 nm and diameters of around 90 nm and depth of about 40 μm. The structure was made by utilizing the anodic oxidation of an aluminum plate [14]. The target was irradiated by a Ti : Al_2O_3 laser pulse with 100 fs pulse duration at the intensity of 1.5×10^{16} W/cm^2. The solid line of Fig. 2 shows the time-integrated soft X-ray spectral fluence from this target and the dotted line shows that from an ordinary flat surface alumina plate target. The intensity

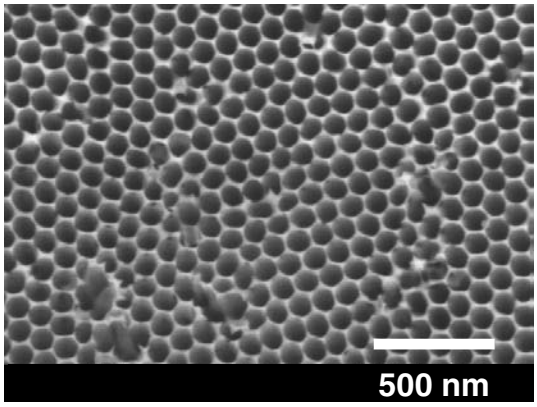

FIGURE 1 Top-view SEM image of an anodic alumina nanohole-array target

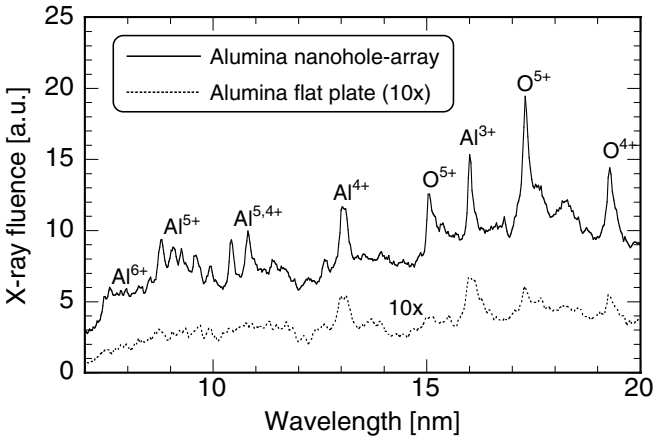

FIGURE 2 Time-integrated soft X-ray spectral fluence from an alumina nanohole-array target

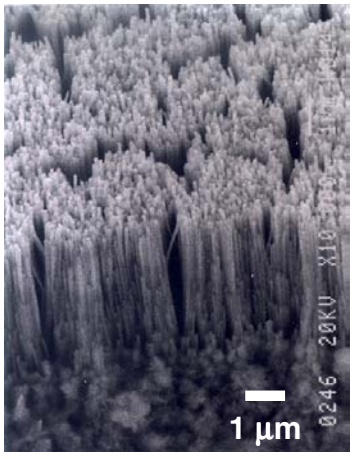

FIGURE 3 Bird's-eye view SEM image of an Au nanocylinder-array target

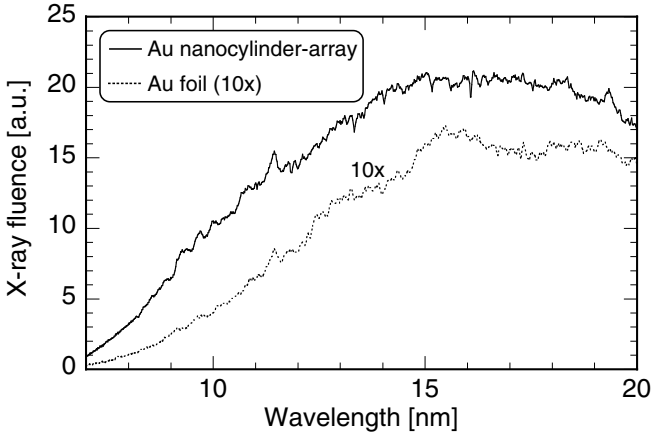

FIGURE 4 Time integrated soft X-ray spectral fluence from an Au nanocylinder-array target

scale on the alumina plate was expanded by a factor of ten. By making an array of nanoholes on the target surface, around a 30-fold X-ray enhancement was obtained in the soft X-ray wavelength region from 7 to 20 nm. X-ray pulse duration was 17 ps.

Figure 3 shows the SEM image of the gold nanocylinder-array target with cylinder diameter of around 80 nm and length of 18 μm. The target was made by filling up the nanoholes of the anodic alumina (hole interval: 100 nm, hole diameter: 70–90 nm) with Au by electrodeposition, then the alumina part was removed [15]. The solid line in Fig. 4 shows the time-integrated soft X-ray spectral fluence from this target and the dotted line shows that from a flat surface gold foil target with thickness of 20 μm. The intensity scale on the gold foil target was expanded by a factor of ten. Large X-ray emission enhancement of around 20-fold was achieved by the Au nanocylinder-array target over the entire soft X-ray wavelength region. Soft X-ray pulse duration on the Au nanocylinder-array target was 17 ps.

Accordingly, these types of targets are effective in enhancing the X-ray intensity even in the soft X-ray energy region while keeping the X-ray pulse duration relatively short compared with other types of targets [1–10]. We have also investigated the required nanostructure size conditions for obtaining efficient X-ray generation with these targets and found that: The nanowall thickness should be less than 100 nm, the nanospace size should be from 100 nm to 1 μm, and the nanostructure depth larger than 10 μm [12].

Unfortunately, alumina and gold do not have intense emission levels in the water-window region. In order to apply this enhancement method in this region, we must chose a target that meets above nanostructure size conditions and that consists of materials with an intense emission level in the water-window region. In this report, we adopted vertically aligned carbon nanotube (CNT) targets [16]. This target meets the nanostructure size requirement, and carbon has intense emission lines in the water-window region. Furthermore, mass pro-

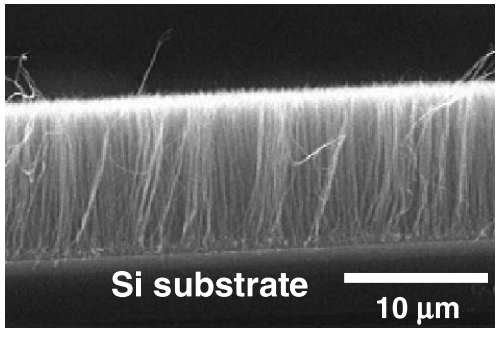

FIGURE 5 Side-view SEM image of the vertically aligned multiwalled carbon nanotube target

duction of CNTs at low cost will be possible, and a target with a large area is obtainable. The target is made by microwave plasma-enhanced chemical vapor deposition [17]. Figure 5 shows a side-view SEM image of the target. Vertically aligned CNTs were formed on a silicon substrate. Each nanotube is multiwalled and about 30 nm in diameter and about 12-μm long. Center-to-center nanotube distance is about 150 nm.

3 Experimental setup

Our laser system consists of a passively mode-locked Ti : Al_2O_3 laser, a pulse stretcher, a regenerative amplifier, a three-pass linear amplifier, and a pulse compressor. The output pulses from the laser system have 100-fs pulse duration with a 10-Hz repetition rate. The wavelength is 790 nm. When using a structured target, a high contrast ratio is necessary in order to ensure an unexpected pre-pulse does not destroy the structure. The contrast ratio between the main pulse and the undesirable child-pulse that precedes it by 3.9 ns is greater than $10^6 : 1$. This was achieved by placing an extra pulse slicer unit behind the regenerative amplifier. The nanostructure of the target remains by irradiation of a 100 fs laser pulse at below the 10^{-6} times the maximum laser intensity. The target was mounted on an *xyz* translation stage in a vacuum chamber and was rastered to expose a fresh surface at each laser shot. Laser pulses from a titanium-sapphire-laser-based amplifier system were focused on the target by using a lens with a focal length of 200 mm at normal incidence. The focused spot size was about 30 μm. The soft X-ray spectrum of the water-window region was measured with a flat-field grazing-incidence spectrograph (nominal groove number: 2400 lines/mm) mounted after a nickel-coated toroidal mirror. X-ray pulse shapes were measured with an X-ray streak camera (time resolution: 3 ps) mounted after a platinum-coated toroidal mirror. Both measurements were done in a single-laser-shot measurement at a 45 degree angle to the target normal.

4 Water-window spectrum

Figure 6 shows the time-integrated X-ray spectrum from a carbon plate and several types of CNT targets in the water-window region when the incident laser pulse energy and the peak intensity on the target was 43 ± 5 mJ and $(3.7 \pm 0.4) \times 10^{16}$ W/cm^2 respectively. The data from three single-shot-measurements were accumulated. *K*-shell resonance lines from the helium-like carbon ions He_α and He_β and from the hydrogen-like carbon ions (Ly_α, Ly_β, and Ly_γ) are observed. The X-ray intensity becomes higher in the order of the carbon plate, unaligned single-walled CNTs, unaligned multiwalled CNTs, and vertically aligned multiwalled CNTs. The X-ray intensity from the multiwalled CNT target is higher than that from the single-walled CNT target. This difference comes from the CNT's diameter. The diameter of the multiwalled CNTs is around 30 nm. This value is similar to the femtosecond laser interaction skin depth [18] and adequate for forming nanometer-sized spaces and a low-average-density but a high local density structure, which are suitable for efficient laser matter interaction [13]. On the other hand, the diameter of the single-walled CNTs is about 1.4 nm, and therefore adequate nanometer-sized spaces for confining

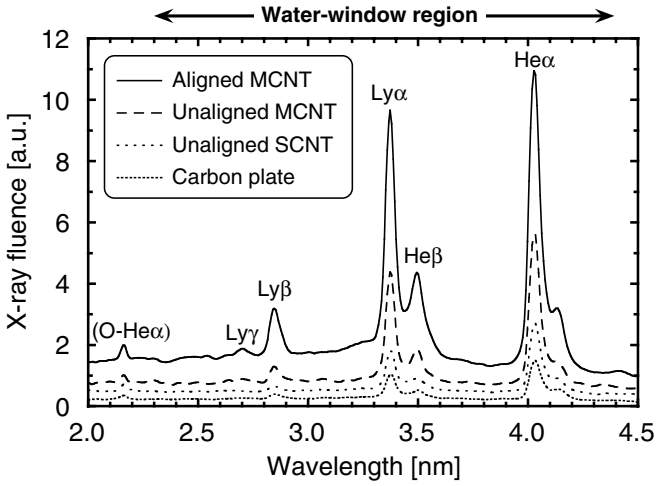

FIGURE 6 Time-integrated X-ray spectral fluence in the water-window region from vertically aligned multiwalled CNT (aligned MCNT), unaligned multiwalled CNT (unaligned MCNT), unaligned single-walled CNT (unaligned SCNT), and carbon plate targets

plasma can not be constructed. It is also found that the X-ray intensity becomes higher when the CNTs are aligned to the direction of laser incidence. In case of a oblique incidence of laser light with a vertically aligned nanocylinder target, X-ray emission intensity was decreased. We think these alignment to the laser incident direction results in increased laser interaction depth. By employing vertically aligned multiwalled CNT target, we achieved enhancements of sevenfold in the water-window region, 7.5-fold at the He_α line (4.0 nm), and ninefold at the Ly_α line (3.4 nm), compared with a conventional carbon plate target.

X-ray pulse generation characteristics in the water-window region from laser-produced plasma have been investigated in detail for a carbon plate target by Altenbernd et al. [19]. Based on their results, the total X-ray emission integrated over the water-window region (2.3–4.4 nm) from a carbon plate target at incident laser pulse conditions similar to those in our experiment was 20 nJ/(sr μm^2) per pulse. Accordingly, the total X-ray emission from our multiwalled CNT target integrated over the water-window region is estimated as 140 nJ/(sr μm^2) per pulse. This corresponds to 2×10^{17} photons/(sr cm^2) per pulse. Assuming the X-ray emission area is same as the illuminated laser spot size, we calculated the total photon number as 2×10^{12} photons/sr per pulse.

5 Incident laser intensity dependence

Figure 7 shows the incident laser peak intensity dependence of soft X-ray fluence integrated over the water-window region. In the case of the carbon plate target (the open circles), soft X-ray fluence rapidly dropped when the laser intensity was lower than 1×10^{16} W/cm^2. On the other hand, no such tendency was observed for the vertically aligned multiwalled CNT target (the closed circles). More than tenfold soft X-ray fluence can be obtained in the low incident laser intensity region and sixfold fluence can be obtained even at the highest incident laser intensity. Also noteworthy is that, by using the CNT target, the same soft X-ray intensity can

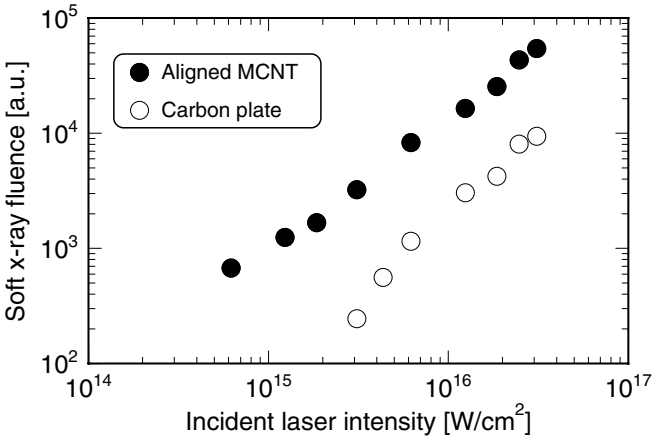

FIGURE 7 Incident laser intensity dependence of soft X-ray fluence integrated over the water-window region from vertically aligned multiwalled CNT (*closed circles*) and carbon plate (*open circles*) targets

be obtained with less than one-fourth the laser intensity even in the highest laser intensity region. This is very beneficial for practical use. For example, a compact mJ class laser system with a kHz repetition rate becomes available for plasma production.

Figure 8 shows the incident laser peak intensity dependence of the carbon He $_\alpha$ line intensity and the carbon Lyman-α (Ly$_\alpha$) line intensity obtained by a single-shot measurement. When the incident laser pulse intensity is low, the line intensity from hydrogen-like ions (Ly$_\alpha$) is much lower than that from He-like ions (He $_\alpha$). However, the intensity difference becomes smaller as the incident laser pulse intensity increases. This means that the plasma temperature becomes higher as the incident laser intensity increases. It is also found that even when the incident laser intensity is the same, the intensity difference between the hydrogen-like line and the He-like line from the vertically aligned multiwalled CNT target is smaller than that from the carbon plate target. This indicates that, by using the CNT target instead of a carbon plate target, higher plasma temperature can be achieved at the same laser intensity. This is because the carbon nanotubes can be heated almost throughout since the carbon nanotube diameter is smaller than the laser skin depth, and thereby plasma cooling due to heat conduction into the underlying cold bulk is suppressed.

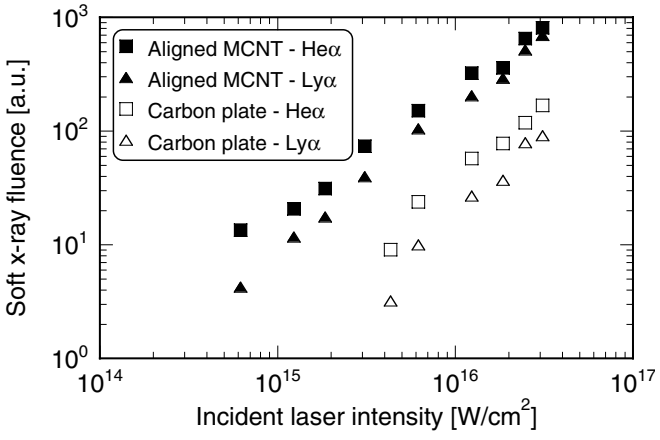

FIGURE 8 Incident laser intensity dependence of the carbon He$_\alpha$ line intensity and the carbon Lyman-α (Ly-α) line intensity from vertically aligneg multiwalled CNT (*closed marks*) and carbon plate (*open marks*) targets

6 Soft X-ray pulse shapes

Generated soft X-ray pulse shapes were measured with an X-ray streak camera equipped with a CsI photocathode (time resolution: 3 ps), which was mounted after a platinum-coated toroidal mirror. The observed X-ray spectral region determined by the reflectivity of the toroidal mirror and the sensitivity of the photo-cathode was 0.05 to 1.5 keV. The solid line of Fig. 9 is the soft X-ray pulse shape obtained from the vertically aligned multiwalled CNT target and the dotted line is that from a carbon plate target. The incident laser intensity was $(3.7 \pm 0.4) \times 10^{16}$ W/cm^2. The data from five single-shot measurements were accumulated. Soft X-ray pulse duration on the CNT target was 26 ps, while pulse duration on the carbon plate target was 8 ps. The nanometer-sized spaces and lower heat conductivity of the CNT target structure result in this threefold increase in the X-ray pulse duration [12]. However, because of the high-local-density structure, the X-ray pulse duration is still much shorter than that obtained using the pre-pulse technique, which is around 100 ps [20, 21].

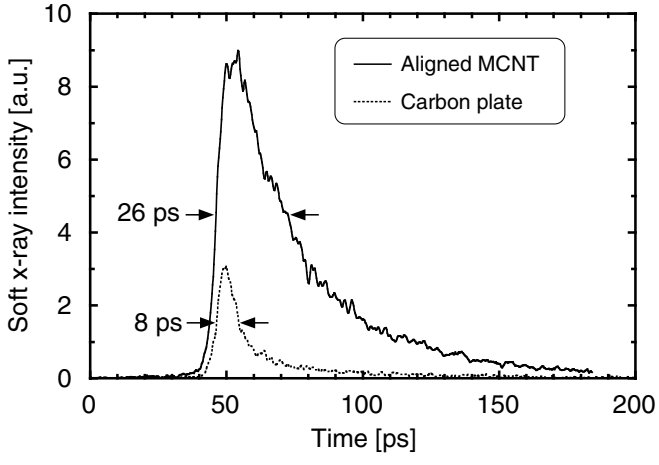

FIGURE 9 Soft X-ray (0.05–1.5 keV) pulse shapes generated from vertically aligned multiwalled CNT (*solid line*) and carbon plate (*dotted line*) targets

7 Water-window X-ray microscopy

The obtained photon number in the water-window region with our target is estimated as 2×10^{17} photons/(sr μm^2) per pulse. In order to achieve the desired spatial resolution in X-ray microscopy, a certain X-ray dose must be absorbed by the specimen. There is no significant difference in the absorbed doses among the different imaging methods, i.e., absorption contrast, phase contrast, and holography [22]. Considering an application of our X-ray source for imaging X-ray microscopy, 10^{14} photons/cm^2 could be achieved on the sample when the X-ray optics meet following conditions: collected solid angle is 0.1 msr, reflectivity is 50%, and magnification on the sample is three. The

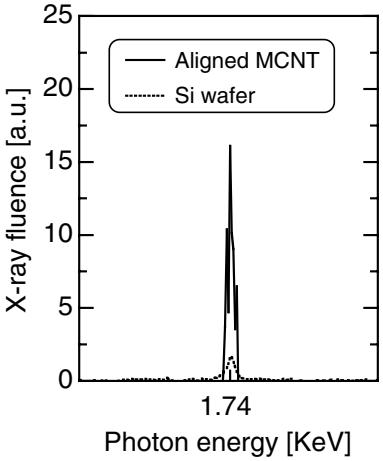

FIGURE 10 Time-integrated Si K_α X-ray spectral from Si substrate of the vertically aligned multiwalled CNT target (*solid line*) and a Si wafer target (*dotted line*)

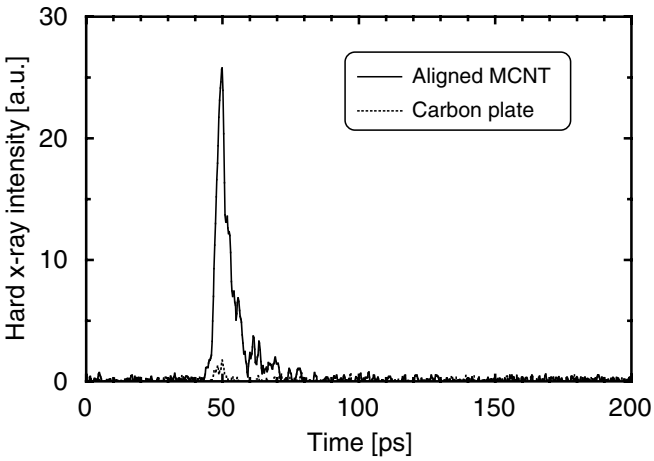

FIGURE 11 Hard X-ray (0.7–2 keV) pulse shapes generated from vertically aligned multiwalled CNT (solid line) and carbon plate (dotted line) targets

illumination of 10^{14} photons/cm^2 during imaging approximately corresponds to the absorbed dose of 10^5 Gy [23]. This value meets the dose requirement for achieving 50-nm image resolution [22]. By optimizing the size of the carbon nanotubes, further X-ray generation enhancement can be expected. Therefore, higher resolution will be available. The absorbed doses result in hydrodynamic motion of the specimen. The image must, therefore, be taken before these structural changes cause blurring of the image. London et al. have estimated the required maximum exposure times for obtaining certain spatial resolution [24]. According to their estimation, 40-nm resolution can be achieved using an X-ray pulse of 26 ps duration when the X-ray dose is sufficient. These results indicate that carbon nanotubes are very attractive as a target of the femtosecond laser-produced-plasma X-ray source in single-shot X-ray microscopy.

8 K_α emission enhancement

Carbon nanotubes are also useful for enhancing K_α emission from laser produced plasma X-ray sources. The keV photon energy region spectrum was measured with a spherically bent mica crystal ($2d = 1.99$ nm) with a bending radius of 100 mm and a back illuminated X-ray CCD camera which are placed after two 10 μm Be filters. The solid line of Fig. 10 shows the Si K_α X-ray line emission from Si substrate of the carbon nanotube target. The dotted line shows that from a bare Si wafer target. The incident laser intensity was $(3.7\pm0.4) \times 10^{16}$ W/cm^2. By covering a solid Si with carbon nanotubes, the Si K_α line emission was enhanced. The mechanism can be explained as follows. Fast electrons are generated effectively from the carbon nanotube part with nanostructure effects [9], and they penetrate into the Si substrate to generate intense K_α X-ray pulses.

In order to also measure the X-ray pulse shape in the keV energy range, a 10 μm Be filter was added in front of the X-ray streak camera. The observable X-ray spectral region was from 0.7 to 2 keV. The solid line of Fig. 11 is the hard X-ray pulse shape obtained from the vertically aligned multiwalled CNT target and the dotted line is that from a carbon plate target. Unlike the case of the soft X-ray region, no manifest expansion of the pulse duration was observed within the resolution limit of the streak camera (3 ps).

These results indicate that by covering various solid materials with carbon nanotubes, enhanced K_α X-ray emission with the corresponding wavelength can be obtained while keeping the X-ray pulse duration short.

9 Summary

By using vertically aligned multiwalled carbon nanotubes as the target of a femtosecond laser-produced-plasma X-ray source, we obtained intense short X-ray pulses in the water-window region. A sevenfold X-ray fluence enhancement was achieved compared with a conventional carbon plate target, and the obtained photon number in the water-window region is estimated as 2×10^{12} photons/sr per pulse. The X-ray pulse duration integrated over from 0.05 to 1.5 keV was 26 ps. Further X-ray generation enhancement can be expected by optimizing the size of the carbon nanotubes. With the large photon number and short X-ray pulse duration, 50-nm spatial resolution can be achieved in the single-shot X-ray microscopy. Carbon nanotubes are also useful for obtaining enhanced K_α X-ray emission from various materials. In the near future, low-cost mass production of CNT targets will be possible. These results indicate that carbon nanotubes are very attractive as a target of the femtosecond laser-produced-plasma X-ray source in single-shot X-ray microscopy and time-resolved X-ray diffraction.

REFERENCES

1 M.M. Murnane, H.C. Kapteyn, S.P. Gordon, R.W. Falcone: Appl. Phys. B **58**, 261 (1994)
2 S.P. Gordon, T. Donnelly, A. Sullivan, H. Hamster, R.W. Falcone: Opt. Lett. **19**, 484 (1994)
3 C. Wülker, W. Theobald, D.R. Gnass, F.P. Schäfer, J.S. Bakos, R. Sauerbrey, S.P. Gordon, R.W. Falcone: Appl. Phys. Lett. **68**, 1338 (1996)
4 T. Nishikawa, H. Nakano, H. Ahn, N. Uesugi, T. Serikawa: Appl. Phys. Lett. **70**, 1653 (1997); T. Nishikawa, H. Nakano, N. Uesugi, T. Serikawa: Appl. Phys. B **66**, 567 (1998)
5 R.V. Volkov, V.M. Gordienko, M.S. Dzhidzhoev, B.V. Kamenev, P.K. Kashkarov, Yu.V. Ponomarev, A. B. Savel'ev, V.Yu. Timoshenko, A.A. Shashkov, Quantum Electronics **28**, 1 (1998)

6 G. Kulcsár, D. AlMawlawi, F.W. Budnik, P.R. Herman, M. Moskovits, L. Zhao, R.S. Marjoribanks: Phys. Rev. Lett. **84**, 5149 (2000)
7 T. Nishikawa, H. Nakano, N. Uesugi: *X-ray Lasers 1998, Inst. Phys. Conf. Ser. 159*, (Institute of Physics Publishing, p. 539 (1999)
8 Y. Hironaka, Y. Fujimoto, K. Nakamura, K. Kondo, M. Yoshida: Appl. Phys. Lett. **74**, 1645 (1999)
9 R.V. Volkov, D.M. Golishnikov, V.M. Gordienko, P.M. Mikheev, A. B. Savel'ev, V. D. Sevast'yanov, V.S. Chernysh, O.V. Chutko, JETP Lett. **72**, 401 (2000); R.V. Volkov, S.A. Gavrilov, D.M. Golishnikov, V.M. Gordienko, P.M. Mikheev, A. B. Savel'ev, A.A. Serov, Quantum Electronics **31** 241 (2001)
10 P.P. Rajeev, S. Banerjee, A.S. Sandhu, R.C. Issac, L.C. Tribedi, G.R. Kumar: Phys. Rev. A **65**, 052 903 (2002); P.P. Rajeev, P. Taneja, P. Ayyub, A.S. Sandhu, G.R. Kumar: Phys. Rev. Lett. **90**, 115 002 (2003)
11 T. Nishikawa, H. Nakano, N. Uesugi, M. Nakao, H. Masuda: Appl. Phys. Lett. **75**, 4079 (1999)
12 T. Nishikawa, H. Nakano, N. Uesugi, M. Nakao, K. Nishio, H. Masuda, *X-ray Lasers 2002, AIP Conference Proceedings 641* (American Institute of Physics, New York, pp. 455 (2002)
13 T. Nishikawa, H. Nakano, K. Oguri, N. Uesugi, M. Nakao, K. Nishio, H. Masuda: Appl. Phys. B **73**, 185 (2001)
14 H. Masuda, K. Fukuda: Science **268**, 1466 (1995); H. Masuda, F. Hasegawa, S. Ono, J. Electrochem. Soc. **144** L127 (1997)
15 H. Masuda, H. Tanaka, N. Baba, Bull. Chem. Soc. Jpn. **66**, 305 (1993); H. Masuda, M. Yotsuya, M. Ishida: Jpn. J. Appl. Phys. **37** L1090 (1998)
16 T. Nishikawa, K. Oguri, S. Suzuki, Y. Watanabe, O. Zhou, H. Nakano: Jpn. J. Appl. Phys. **42** L990 (2003)
17 C. Bower, W. Zhu, S. Jin, O. Zhou: Appl. Phys. Lett. **77**, 830 (2000); C. Bower, O. Zhou, W. Zhu, D.J. Werder, S. Jin: Appl. Phys. Lett. **77**, 2767 (2000)
18 A. Zigler, P.G. Burkhalter, D.J. Nagel, M.D. Rosen, K. Boyer, G. Gibson, T.S. Luk, A. McPherson, C.K. Rhodes: Appl. Phys. Lett. **59**, 534 (1991)
19 D. Altenbernd, U. Teubner, P. Gibbon, E. Förster, P. Audebert, J.P. Geindre, J.C. Gauthier, G. Grillon, A. Antonetti: J. Phys. B: At. Mol. Opt. Phys. **30**, 3969 (1997)
20 H. Nakano, T. Nishikawa, H. Ahn, N. Uesugi: Appl. Phys. Lett. **69**, 2992 (1996)
21 H. Nakano, P. Lu, T. Nishikawa, N. Uesugi: *X-ray Lasers 1998, Inst. Phys. Conf. Ser. 159* (Institute of Physics Publishing, p. 535 (1999)
22 K. Shinohara, A. Ito: J. Microscopy **161**, 463 (1991)
23 A. Ito, K. Shinohara: Cell Structure Function **17**, 209 (1992)
24 R.A. London, M.D. Rosen, J.E. Trebes: Appl. Opt. **28**, 3397 (1989)